

A synthetic–natural hybrid oscillator in human cells

Jared E. Toettcher^{a,b}, Caroline Mock^a, Eric Batchelor^a, Alexander Loewer^a, and Galit Lahav^{a,1}

^aDepartment of Systems Biology, Harvard Medical School, Boston, MA 02115; and ^bDepartment of Biological Engineering, Massachusetts Institute of Technology, Cambridge, MA 02139

Edited by Charles S. Peskin, New York University, and approved August 17, 2010 (received for review April 28, 2010)

Recent studies have shown that many cell-signaling networks contain interactions and feedback loops that give rise to complex dynamics. Synthetic biology has allowed researchers to construct and analyze well-defined signaling circuits exhibiting behavior that can be predicted and quantitatively understood. Combining these approaches—wiring natural network components together with engineered interactions—has the potential to precisely modulate the dynamics of endogenous signaling processes and control the cell decisions they influence. Here, we focus on the p53 signaling pathway as a template for constructing a tunable oscillator comprised of both natural and synthetic components in mammalian cells. We find that a reduced p53 circuit implementing a single feedback loop preserves some features of the full network's dynamics, exhibiting pulses of p53 with tightly controlled timing. However, in contrast to the full natural p53 network, these pulses are damped in individual cells, with amplitude that depends on the input strength. Guided by a computational model of the reduced circuit, we constructed and analyzed circuit variants supplemented with synthetic positive and negative feedback loops and subjected to chemical perturbation. Our work demonstrates that three important features of oscillator dynamics—amplitude, period, and the rate of damping—can be controlled by manipulating stimulus level, interaction strength, and feedback topology. The approaches taken here may be useful for the rational design of synthetic networks with defined dynamics, and for identifying perturbations that control dynamics in natural biological circuits for research or therapeutic purposes.

live-cell imaging | oscillations | systems biology | mathematical modeling

Cell-signaling networks sense and encode dynamic information. Biochemical oscillators ensure the proper timing of events in periodic processes (1, 2), and transient or sustained activation of signaling proteins can affect cell-fate decisions (3). Because these decisions must be precisely organized in time and space, specific features of the dynamics, such as the timing or amplitude of a pulse, must be tightly controlled. Thus, understanding how feedback loops and other interactions in biological networks determine their dynamics (4) and how these dynamics can be perturbed are central challenges of systems biology.

One approach for understanding how biological networks give rise to specific dynamics is to synthetically engineer simple circuits with well-defined dynamic behaviors (for example, ref. 5). This approach has been applied to transcriptional oscillators, an important class of biological networks. Synthetic oscillators have been engineered in bacteria using negative feedback loops (6) or combinations of negative and positive feedback loops (7, 8). Such synthetic networks were also recently demonstrated in mammalian cells (9). However, these synthetic oscillators were constructed using elements completely foreign to the cell. Networks composed of both natural and artificial elements can be useful in characterizing the dynamic features of natural systems in a controlled way and in modulating the dynamics of natural signaling proteins to exert fine control over a cell's response (10). For example, replacing natural regulation with artificial components highlighted recently the importance of noise in the bacterial competence network (11). Here, we address the challenge of constructing a hybrid synthetic–natural oscillator using components of the p53 signaling network.

p53 is a transcription factor activated in response to cellular stresses, such as DNA damage (12). It activates stress response programs such as apoptosis and cell cycle arrest, and it also regulates targets that modulate its own activation or stability, forming multiple positive and negative feedback loops (13). One of the best-characterized feedback loops acts through the E3 ubiquitin ligase Mdm2; p53 induces *mdm2* transcription and Mdm2 protein targets p53 for degradation (14). Cellular stress activates upstream kinases that posttranslationally modify p53 and Mdm2 and disrupt the p53–Mdm2 interaction, stabilizing p53 and modulating its transcriptional activity.

p53 has been shown to undergo complex dynamics in response to γ -irradiation (IR) (15, 16). After IR, individual cells show a series of p53 pulses characterized by tight control over three distinct dynamic features. First, the pulse amplitude does not depend on the IR dose. Second, the pulses are undamped; the mean amplitude of successive pulses remains constant. Finally, although pulse amplitude can be highly variable between individual cells, the timing of pulses is tightly controlled (16). In our previous work, we showed that the simple p53–Mdm2 feedback loop is insufficient in explaining these features of the dynamics, and that the p53 pulses are driven by pulses in the kinases ATM and Chk2, which participate in additional feedbacks with p53 through the Wip1 phosphatase (Fig. 1A) (17, 18).

Here, we report the construction of synthetic variants of the p53 circuit based on transcriptional stimulation of p53 and its negative regulator, Mdm2. This reduced network does not include the kinases ATM/Chk2, providing a more tractable system for analysis and manipulation. We find that the simple core p53–Mdm2 negative feedback loop undergoes tightly controlled oscillations that share a subset of the features of the IR response. However, in contrast to the full network activated by IR, synthetic activation of the p53–Mdm2 loop generates damped oscillations with pulse amplitudes that depend on the input dose. We constructed and analyzed a mathematical model of this circuit to identify perturbations that could alter specific features of p53's oscillatory behavior. We then tested these predictions experimentally and showed that the damping rate of p53 oscillations can be modulated by additional synthetic positive and negative feedback loops on p53 and the oscillation frequency can be tuned by varying the feedback strength of the p53–Mdm2 loop. This study shows that we can “plug in” to existing elements within human cells and accurately control specific features of their dynamics. It also suggests tools for perturbing specific features of dynamics (e.g., amplitude, period, and damping) of additional oscillators in human cells in a controlled way, a crucial step toward understanding the role they play in signaling pathway responses.

Author contributions: J.E.T. and G.L. designed research; J.E.T. and C.M. performed research; J.E.T., E.B., and A.L. contributed new reagents/analytic tools; J.E.T., C.M., and G.L. analyzed data; and J.E.T., C.M., and G.L. wrote the paper.

The authors declare no conflict of interest.

This article is a PNAS Direct Submission.

¹To whom correspondence should be addressed. E-mail: galit@hms.harvard.edu.

This article contains supporting information online at www.pnas.org/lookup/suppl/doi:10.1073/pnas.1005615107/-DCSupplemental.

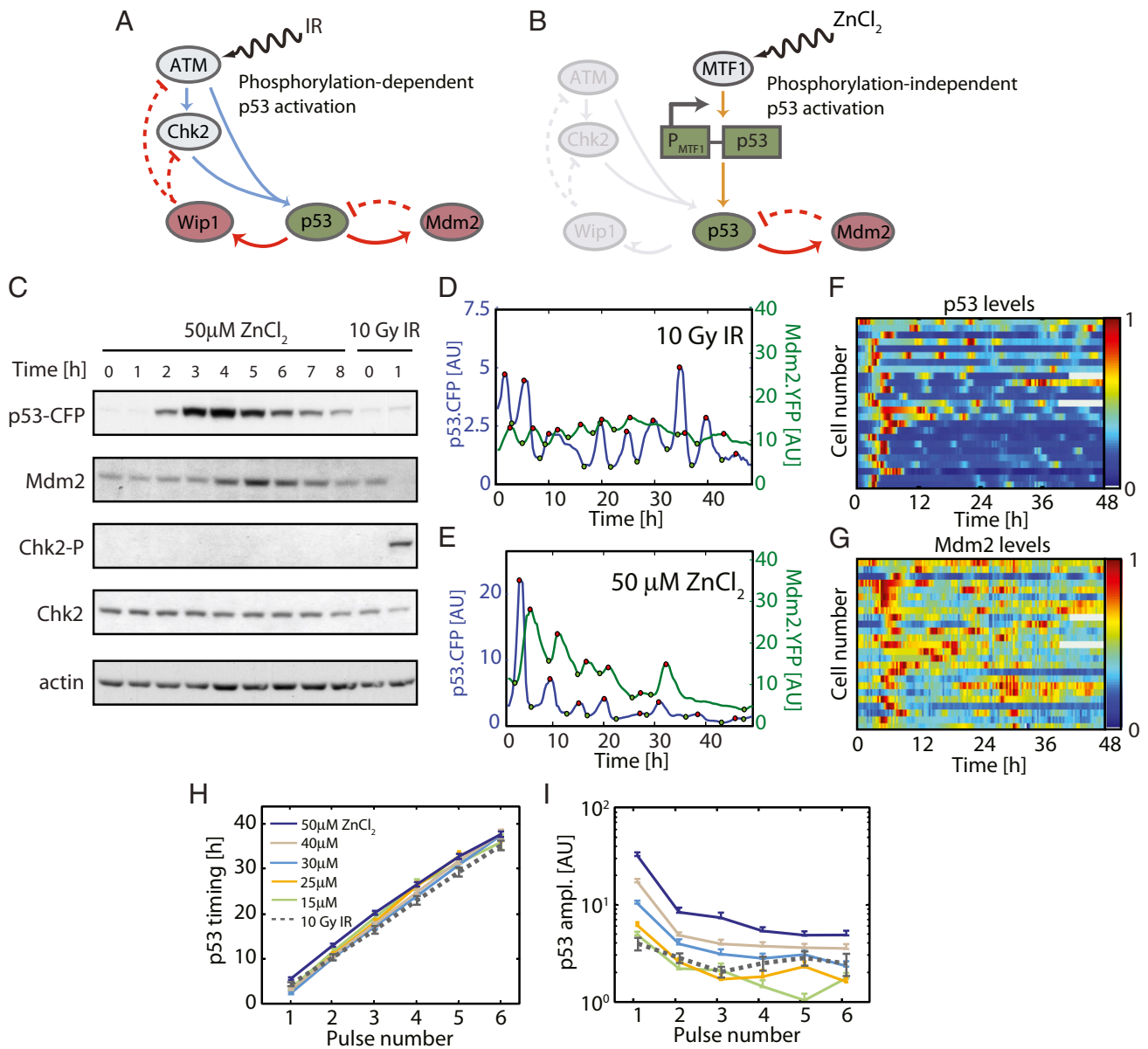


Fig. 1. A reduced p53–Mdm2 circuit generates graded damped oscillations of fixed frequency. (A) Feedbacks regulating p53 dynamics after IR. IR activates ATM and Chk2 phosphorylation, which leads to p53 stabilization. Negative feedbacks act through the Mdm2 ubiquitin ligase to degrade p53, and through the Wip1 phosphatase to inactivate the upstream kinases. (B) A reduced p53 circuit based on transcriptional activation and the p53–Mdm2 feedback loop. Zinc stimulates p53–CFP transcription from a metallothionein (MT) promoter, bypassing IR-induced activation through the ATM/Chk2 kinase cascade and Wip1 negative feedback loop. Induced p53 activates Mdm2 transcription, which negatively regulates p53 stability. (C) Protein levels of p53 and its regulators in response to transcriptional activation of p53. Cells expressing p53–CFP under the MT promoter were treated with 50 μ M zinc or 10 Gy IR, and samples were taken at the indicated time points. Protein levels were analyzed by Western blot, with actin as a loading control. Zinc led to p53 induction followed by Mdm2 induction. Zinc did not affect the level of Chk2 phosphorylation in contrast to activation of the full network by IR. (D and E) Fluorescence intensities of p53–CFP (blue curve) and Mdm2–YFP (green curve) from single cells following IR (D) and transcriptional stimulation by zinc (E). IR (full network) leads to undamped p53 oscillations and zinc induction (p53–Mdm2 core feedback) induces damped oscillations. (F and G) Heat maps of 25 representative cells after 50 μ M zinc treatment. Each row represents a single cell. The p53–CFP (F) and Mdm2–YFP (G) levels were normalized to the maximum amplitude for each cell. (H) p53–CFP pulse timing and (I) fluorescence are shown for each pulse after stimulation with Zinc or IR (mean + SEM computed from at least 50 cells per condition).

Results

Transcriptional Stimulation of the p53–Mdm2 Negative Feedback Generates Damped Oscillations. We first set out to isolate a reduced circuit regulating p53 levels. We used a cell line in which expression of a p53–CFP fusion protein is driven by a zinc-inducible metallothionein promoter (MTp) (15) (Fig. 1B). We found that transcriptional stimulation of the p53–CFP fusion protein by zinc led to a gradual increase in p53–CFP levels in cell populations measured by Western blot, reaching a peak at 4 to 5 h and followed

by a gradual decrease (Fig. 1C and Fig. S1A and B). Induction of p53 by zinc led to an increase in Mdm2 levels (Fig. 1C), demonstrating that synthetic activation of p53 transcription is sufficient to activate the core p53–Mdm2 negative feedback loop even in the absence of cellular stress (19). However, in the absence of IR, feedback loops based on posttranslational modifications [such as the ATM–Chk2–Wip1 loop (17)] were inactive (Fig. 1C). Furthermore, p53–CFP induction using zinc did not induce a cellular stress response, such as cell cycle arrest (Fig. S1C).

We next set out to characterize the dynamics of the core p53–Mdm2 negative feedback loop in individual cells by time-lapse microscopy. We used a previously described cell line expressing zinc inducible p53–CFP and an Mdm2–YFP fusion protein driven by its native promoter (15). Transcriptional stimulation with zinc led to a series of pulses of p53–CFP and Mdm2–YFP in single cells (Fig. 1*E*). Quantitative analysis of single-cell trajectories revealed a synchronous, high amplitude first p53–CFP pulse at about 5 h after induction (Fig. 1*E* and *F*). The corresponding Mdm2–YFP pulse was delayed with respect to the p53–CFP pulse by ≈ 2 h (Fig. 1*E* and *G*).

The pulsatile dynamics observed after artificially inducing transcription of p53–CFP by zinc are reminiscent of those after natural induction following IR (15, 16) (Fig. 1*D*). Specifically, the timing of p53 pulses was tightly controlled with ≈ 5.5 h between consecutive pulses independent of input dose in both conditions (Fig. 1*H* and Fig. S1*D*) (15, 16). This finding suggests that the control of p53 pulse timing may result from an internal property of the p53–Mdm2 feedback loop. Quantitative analysis of the mean amplitude of successive pulses (SI Appendix, “Estimating pulse statistics from trajectories”) revealed two key differences between transcription-induced and IR-induced p53. First, in contrast to the IR response, the amplitude of transcriptionally induced p53–CFP was no longer dose-independent, but rather highly sensitive to zinc concentration (Fig. 1*I*), with a 10-fold difference in first-pulse amplitude between the highest and lowest zinc concentration. Second, successive p53–CFP pulses decrease in amplitude, indicating that, as opposed to IR, individual cells undergo damped oscillations after zinc stimulation (Fig. 1*I*). The fraction of cells with detectable pulses also decreases with pulse number, supporting the observation that these pulses are damped (Fig. S1*E* and *F*). These results show that the simple p53–Mdm2 feedback loop generates a series of dose-dependent damped oscillations and agree with previous

studies, suggesting that additional interactions beyond this core feedback loop are required for generating the undamped digital pulses observed after IR (17).

Modeling the p53–Mdm2 Negative Feedback Circuit. To better understand how different dynamic features in the p53–Mdm2 negative feedback loop may be controlled, we constructed a mathematical model of this simple core circuit. Our model consists of a set of ordinary differential equations representing p53 and Mdm2 (SI Appendix, “Model construction and parameterization”). It incorporates three nonlinear interactions (Fig. S2*A*): Mdm2-mediated ubiquitination of p53 (14), activation of Mdm2 transcription by p53 (20), and autoregulation of Mdm2 stability (21, 22). Each of these three interactions is required to account for a lower dependence of Mdm2 amplitude on zinc concentration and pulse number as observed experimentally (Fig. S2*B–E*).

We parameterized our model of the p53–Mdm2 circuit to match data collected at five zinc concentrations. First, we experimentally measured the transfer function of the transcription factor MTF1 using a cell line in which CFP was placed directly under the control of the metallothionein promoter (Fig. S2*F* and *G*). We next applied a local optimization procedure to fit the simulated p53 and Mdm2 first-pulse amplitudes, frequency, and damping to the experimental measured data (see SI Appendix, “Model construction and parameterization” and Table S1 for computation details). Our fitted model captures the observed p53 dynamics, reproducing the scaling of p53 amplitude across different zinc concentrations and the relatively invariant frequency and damping coefficients (Fig. 2*A–C*, compare experimental datapoints with fitted model lines). As was shown experimentally, the model exhibits a lesser dependence of Mdm2 amplitude on zinc dose than that of p53 (Fig. 2*F*). However, the model predicts more sensitivity of

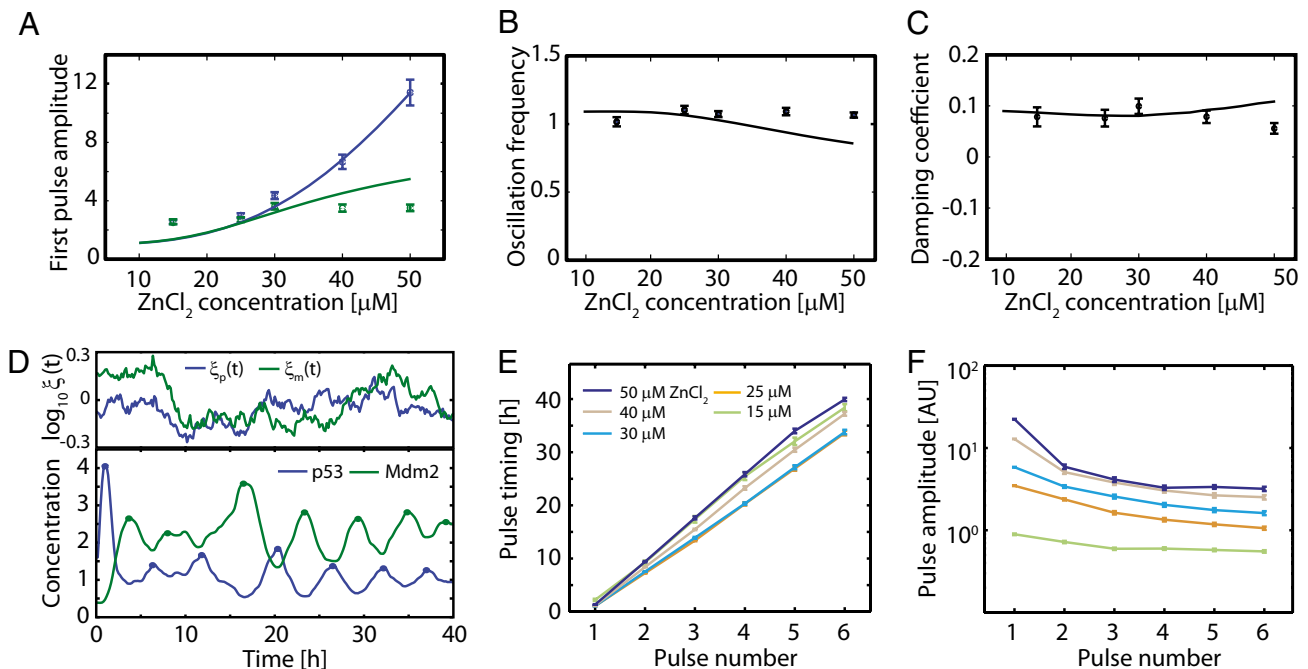


Fig. 2. Mathematical modeling of the core p53–Mdm2 negative feedback circuit. (A–C) A fitted model reproducing p53/Mdm2 dynamics. The p53 (blue) and Mdm2 (green) amplitudes (A), frequency of p53 oscillation (B), and p53 damping coefficient (C) at varying zinc concentrations are shown. The mean amplitude is plotted for each pulse; mean frequency and damping were taken across all pulses. Points represent experimental data from the zinc-stimulated cells shown in Fig. 1*H* and *I* (mean + SEM); curves show model results. (D) Model dynamics in the presence of transcriptional noise. The lower panel shows modeled p53 (blue trace) and Mdm2 (green trace) levels after 25 μM zinc stimulation in the presence of noise in p53 and Mdm2 production. The upper trace shows the corresponding transcriptional noise applied to p53 [$\xi_p(t)$] and Mdm2 [$\xi_m(t)$] (SI Appendix, “Noise simulations”). The p53 timing (E) and amplitude (F) for 100 modeled cells are plotted for each pulse after stimulation (mean + SEM).

Mdm2 amplitude to zinc dose than was experimentally observed (Fig. 24). This result might arise from additional mechanisms of Mdm2 regulation, or might reflect variation in the concentration of other less well understood p53-dependent ubiquitin ligases, such as Cop1 or Pirh2 (23, 24).

In addition to these deterministic simulations, we ran our model in the presence of transcriptional noise (16) to compare the results with the cell population data of Fig. 1 H and I (see *SI Appendix*, “Noise simulations” for details). Fig. 2D shows a representative modeled cell with noise modulating both the p53 and the Mdm2 production rates. We tabulated the p53 amplitude and timing profiles from 100 modeled cells at each of five zinc concentrations. In agreement with our experimental results (Fig. 1 H and I), simulation of 100 cells in the presence of transcriptional noise led to a tightly controlled pulse-timing independent of input dose (Fig. 2E) and to dose-dependent damping amplitude (Fig. 2F).

Synthetic Transcriptional Feedback Loops Modulate Oscillation Damping Rate. The reduced p53–Mdm2 negative feedback loop led to damped oscillations. We next aimed to identify methods for perturbing specific features of these dynamics using our mathematical model. Recent work suggests that a combination of negative and positive feedbacks can lead to robust undamped oscillation and tunable frequency (25, 26). We therefore asked whether additional feedback loops can play similar roles in the context of the core p53–Mdm2 circuit. We reasoned that our input to the p53–Mdm2 negative feedback loop—transcriptional induction of p53–CFP—provides a node at which we can add additional synthetic feedback loops, and we used our model to predict the effects of such feedback connections through either an inducer or repressor of p53 transcription.

We first augmented our model to include p53-mediated induction of additional feedback loops and their corresponding effect on p53, and simulated dynamics for a range of feedback strengths and delay times (see *SI Appendix*, “Modeling synthetic

feedback” and *Table S2* for details). We found that additional feedback loops on p53 only weakly affected oscillation frequency, but had a strong effect on the damping rate (Fig. 3 A and B for damping rate and Fig. S3 for all analyses). Oscillation amplitude was strongly affected at high feedback strengths, but weakly affected at lower values (Fig. S3 B and E). For a broad range of parameter values, addition of a positive feedback (leading to a negative- and positive-feedback circuit, NPF) destabilizes the network leading to lower damping rates, and addition of a second synthetic negative feedback loop (2NF) has the opposite effect.

To experimentally test these predictions, we supplemented the core p53–Mdm2 negative feedback circuit (1 negative feedback, 1NF cells) with additional feedback on p53–CFP transcription (Fig. 3 C and D) using variants of MTF1, the zinc-responsive transcription factor that acts on the metallothionein promoter (27). To generate cells with a synthetic positive feedback loop (NPF cells), we expressed MTF1 fused to mCherry from a p53-dependent promoter. In this circuit, p53 induces MTF1–mCherry, which further induces p53–CFP (Fig. 3C). Similarly, we constructed a circuit with an additional negative feedback loop on p53 (2NF cells) using a dominant-negative MTF1-KRAB protein fused to mCherry to repress p53–CFP transcription (Fig. 3D). Note that the p53-inducible MTF1-KRAB transcriptional repressor is expressed in addition to the constitutive endogenous MTF1, so cells with this synthetic loop would still be expected to initially activate p53 in response to zinc (when MTF1-KRAB levels are low) but negatively regulate p53 during subsequent pulses.

Like the 1NF cells, both NPF and 2NF cells generated pulses of p53–CFP after zinc treatment. We found that the damping rate in the NPF was lower than in the 1NF cells, indicated by the higher amplitude of subsequent pulses (Fig. 3E). Conversely, the 2NF cells exhibit a faster damping rate than the 1NF cells, so that after the third pulse the amplitude was too low to detect and the percentage of cells with detectable pulses was significantly reduced (Fig. S4). For 1NF and NPF cells, which still exhibited long-term pulsing, the timing of subsequent pulses was unaffected (Fig. 3F).

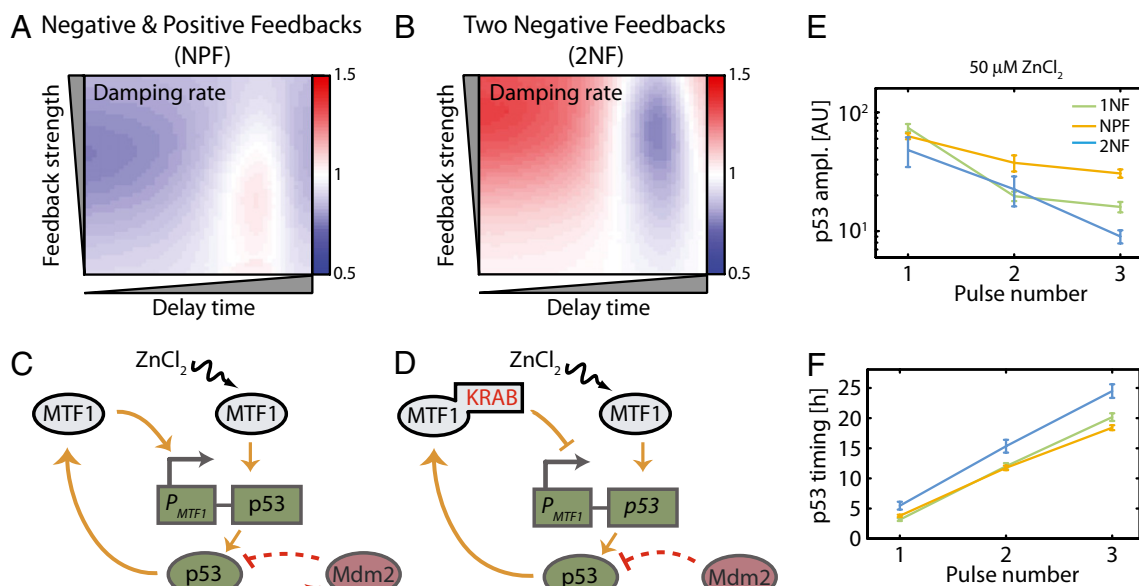


Fig. 3. Model predictions and experimental perturbations for modulating oscillations damping rate. Model predictions for damping rate in a circuit with positive and negative feedbacks (NPF, A) or two negative feedbacks (2NF, B). The x and y axes represent variation of two parameters, γ_{f0} and β_{p0} , across two orders of magnitude, representing feedback protein production delay and its effect on p53 transcription. Color bars show the rate of damping at each point, where white indicates the value from the model without additional feedback. Color scales on each plot range from 50 to 150% of the unperturbed value, permitting relative comparisons between plots. (C and D) Schematics of experimental synthetic feedback systems: (C) A combination of a negative and positive feedbacks on p53; the negative feedback is the natural feedback through Mdm2 (red arrows) and the positive feedback is a synthetic feedback through MTF1 (orange arrows). (D) Two negative feedbacks on p53; one through Mdm2 (red arrows) and the second through MTF1-KRAB (orange arrows). The p53 amplitude (E) and timing (F) measured in 1NF (green), NPF (orange), and 2NF (blue) cells after stimulation with 50 μM zinc.

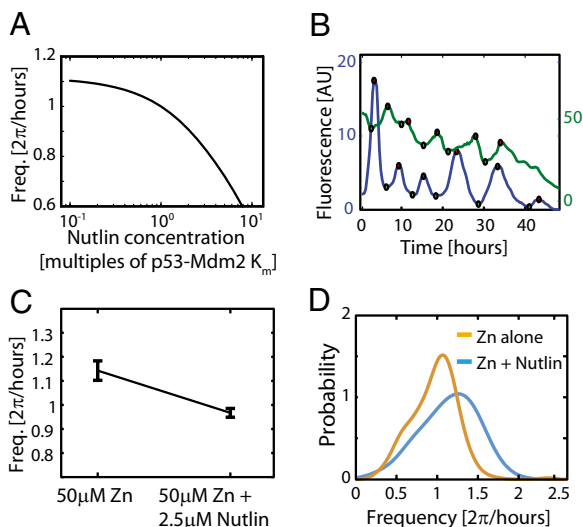


Fig. 4. Model predictions and experimental perturbations for modulating oscillation frequency. (A) Predicted oscillation frequencies in the p53–Mdm2 circuit are plotted against Nutlin3A dose, measured in multiples of its IC₅₀. (B) Representative single-cell trajectories showing p53–CFP (blue trace) and Mdm2–YFP (green trace) after treatment with 50 μM zinc in the presence of 2.5 μM Nutlin3A. (C) Oscillation frequency in nutlin-pretreated cells compared with control cells. (D) Distribution of oscillation frequencies in response to transcriptional induction of p53 by zinc in Nutlin3A-pretreated and control cells.

Together, these results show that the damping rate of the p53–Mdm2 oscillator can be controlled by additional feedback loops acting on p53. Additional positive feedback decreases the damping rate of the p53–Mdm2 oscillator, but additional negative feedback has the opposite effect.

Inhibiting the p53–Mdm2 Interaction Modulates Oscillation Frequency.

One of the distinguishing features of p53 dynamics is the tight regulation of pulse timing. This precise control arises in both the full network in response to IR (15, 16) (Fig. 1 D and H), and in the core p53–Mdm2 circuit activated by zinc (Fig. 1 E and H). We next set out to identify means for controlling the timing of p53 pulses. We used our model to search for interactions in the core p53–Mdm2 circuit that could modulate oscillation frequency by varying each parameter over two orders of magnitude (SI Appendix, “Parameter perturbation analysis” and Figs. S5, S6). Although many of the biological processes associated with sensitive parameters are difficult to modulate experimentally, we could alter the affinity of the p53–Mdm2 interaction using the small molecule Nutlin3A

(28). Computational predictions of the effect of Nutlin3A on oscillation frequency indicated that a concentration 10-fold higher than its IC₅₀ should decrease the frequency by ≈30% (Fig. 4A).

To test this prediction, we preincubated cells with Nutlin3A for 24 h before stimulating them with zinc and followed p53–CFP and Mdm2–YFP levels. We found that cells still oscillate but with longer-duration, lower-frequency pulses (compare Figs. 4B and 1E). We observed an ≈20% decrease in the mean oscillation frequency in Nutlin3A pretreated cells (Fig. 4C). We calculated the distribution of pulse frequencies in cells with or without Nutlin3A pretreatment (Fig. 4D), and found a significant difference in frequency between the two cell populations, (*P* value < 10^{−6} by the Kolmogorov–Smirnov test). These results show that, as predicted by our model, varying the affinity between p53 and Mdm2 proteins “breaks” the tightly controlled timing of p53 oscillations and decreases their frequency.

Conclusions

We have described how individual interactions tune each of three distinct dynamic features of the p53 network. Manipulating the transcriptional rate of p53 using an inducible promoter tunes the amplitude of oscillation without affecting oscillation frequency or damping rates. Synthetic transcriptional feedback loops on p53 can modulate damping with a less-pronounced effect on amplitude and frequency. Finally, targeted perturbation of the p53–Mdm2 interaction tunes oscillation frequency. Taken together, these results show that even a “simple” oscillatory network motif—the delayed negative feedback loop—provides a platform allowing the independent variation of crucial dynamical features.

Two major thrusts of systems biology are the better understanding of the operation of complex natural networks and the de novo design of simple networks. Studying simple core network motifs in isolation offers the greatest potential for manipulating their behavior, but may not offer insight into the complex natural context (Fig. 5A, Left). At the other extreme, natural biological systems can weave many layers of regulation on top of the core signaling pathway, making them hard to understand and to manipulate (Fig. 5A, Right). We suggest that taking a “middle road,” stimulating the pathway in its native context using nonnatural inputs and feedback loops, can help to quantitatively understand and perturb the full system (Fig. 5A, Center).

To illustrate the connection between hybrid and natural systems, we asked whether our work to modulate pulse frequency in the reduced p53 network could be generalized to the p53 pathway in response to ionizing radiation. One of the striking features of p53 oscillations in response to DNA damage is their tightly regulated frequency across IR dose (15–17). No perturbations to date have been shown to alter this frequency. Our computational and experimental results suggest that the frequency might be altered by perturbing the p53–Mdm2 interaction (Fig. 4C and D). Indeed, we found that pretreatment of irradiated cells with Nutlin3A changes

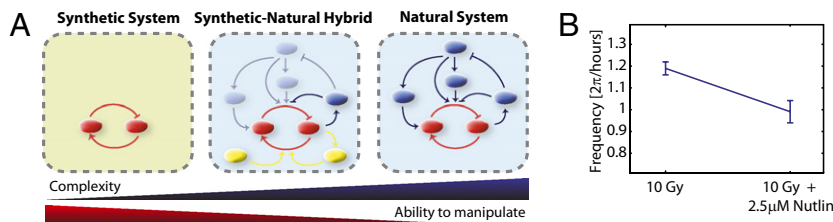


Fig. 5. Synthetic–natural hybrid systems can provide insights into the full network. (A) A synthetic circuit (Left) is constructed from a small number of components (red nodes) in an isolated context. Although easy to manipulate, such circuits are often too distinct from natural biological networks and therefore might provide limited insights. A complete natural system (Right) is highly interconnected and complex. A synthetic–natural hybrid system (Center) includes a reduced number of interactions (faded blue nodes/arrows are not activated) in their natural context (blue background) supplemented by artificially engineered feedbacks (yellow nodes). Such systems are less complicated than full networks, but can be perturbed in a controlled way and are thus useful for developing insights and predictions about the behavior of the full natural network. (B) Oscillation frequency in cells irradiated with 10 Gy IR, and in 10 Gy IR-irradiated cells pretreated with 2.5 μM Nutlin3A. Perturbation of the p53/Mdm2 interaction by Nutlin3A reduces the frequency of p53 oscillations in response to DNA damage.

the frequency of p53 oscillations in response to DNA damage (Fig. 5B). This finding now presents a unique opportunity for investigating whether information is encoded in the frequency of p53 oscillations, as was shown recently in other oscillating systems (29). In addition, the computational and experimental strategy described here provides a set of tools for perturbing the dynamics of other oscillating networks in human cells to enable future investigation of the function of their dynamics, and perhaps to restore a proper dynamic response in cases where it has been deregulated.

Materials and Methods

Cell Lines and Expression Constructs. We used a clonal MCF7 cell line expressing MTP-p53-CFP and Mdm2p-MDM2-YFP as described (15). To create the NPF and 2NF plasmids, Mdm2p-MTF1-mCherry, and Mdm2p-MTF1-KRAB-mCherry, we used the MultiSite-Gateway recombination system (Invitrogen). The human Mdm2 promoter (15), the MTF1 and MTF1-KRAB cDNA (27), and mCherry (30) were cloned into a modified pDEST4R3 vector containing the puromycin resistance gene according to the manufacturer's instructions (Invitrogen). After transfection into the MCF7 cell line containing MTP-p53-CFP and Mdm2p-MDM2-YFP (FuGene6, Roche) (15), cells were selected with puromycin and clonal populations were obtained by single-cell dilution.

Cell lines were grown at 37 °C in RPMI medium supplemented with 10% FBS, 100 U/mL penicillin, 100 µg/mL streptomycin, 250 ng/mL amphotericin B, and appropriate selective antibiotics: G418 (0.4 mg/mL), hygromycin (100 µg/mL), or puromycin (0.5 µg/mL).

Time-Lapse Microscopy. Two days before microscopy, cells were plated onto poly-D-lysine-coated glass bottom plates (MatTek Corporation). One day before microscopy, the media was changed to RPMI lacking riboflavin and phenol red supplemented with 2 to 5% FBS and antibiotics to minimize autofluorescence. Cells were viewed with two types of inverted fluorescence microscope systems, named FMS1 and FMS2. Each system is surrounded by an enclosure to maintain constant temperature, CO₂ concentration, and humidity. FMS1 consists of a Nikon Eclipse-TI-E perfect-focus inverted microscope with a cooled CCD camera Hamamatsu Orca-R2. Brightfield, CFP, YFP, and mCherry images were taken every 20 min using a Prior Lumen 200 metal arc lamp. FMS2 consists of a Nikon Eclipse TE2000-E inverted microscope with a cooled CCD camera Hamamatsu Orca-ER. CFP and YFP images were taken every 20 min with a mercury lamp. CFP filter set: 436 nm/20 nm; 455-nm dichroic beam splitter, and 480-nm/40-nm emission. YFP filter set:

500-nm/20-nm excitation, 515-nm dichroic beam splitter, and 535-nm/30-nm emission (Chroma). The mCherry filter set: 560 nm/40-nm excitation, 585-nm dichroic beam splitter, and 630-nm/75-nm emission (Chroma). Images were acquired using MetaMorph software (Molecular Devices) for 48 h.

Cell Tracking and Fluorescence Quantification. Cell nuclei in the brightfield images were tracked manually in every frame using ImageJ (National Institutes of Health). Mean nuclear fluorescence intensity was measured using custom written MATLAB software (Mathworks Inc.), which measured and subtracted each image background fluorescence and excluded nucleolar regions from each tracked nucleus. Because of autofluorescence caused by the rounding up of cells near times of cell division, the fluorescence signal was masked and interpolated for 2 h before and after cell-division events.

Data Processing and Automated Pulse Identification. Trajectories were smoothed by Blaise filtering as described in refs. 16 and 17. To identify pulse maxima and minima, trajectories were processed by reducing the depth of local minima by 0.2 fluorescence units and performing the morphological opening operation with a width of three time-points to exclude short, noisy fluctuations in amplitude. Maxima were identified from the processed trajectories using the watershed algorithm; minima were identified using the watershed algorithm on the negative reflection of the processed trajectory. For all data analysis, we followed the dynamics of only a single daughter cell after each cell-division event to avoid bias arising from correlations between daughter cells.

Computational Methods. For all simulations, numerical integration was performed in MATLAB using ordinary differential equations 15s (The Mathworks). All computational analyses were carried out using custom written software in MATLAB, which is available upon request.

ACKNOWLEDGMENTS. We thank Bruce Tidor, David Nelson, Kyle Karhohs, Julia Liu, and all members of our laboratory for comments and discussions; Jennifer Waters (Nikon Imaging Center at Harvard Medical School) for advice on live-cell imaging; Walter Schaffner (University of Zurich) for the MTF and MTF1-KRAB cDNAs; and Roger Tsien (University of California, San Diego) for the mCherry expression plasmid. This research was supported in part by National Institutes of Health Grant GM083303, the American Cancer Society (E.B.), the California Division Pamela and Ed Taft Postdoctoral Fellowship (E.B.), and fellowships from the German Research Foundation and the Charles A. King Trust (A.L.).

- Mitchison J (1971) *The Biology of the Cell Cycle* (Cambridge University Press, Cambridge).
- Dunlap J, Loros J, Decoursey P (2004) *Chronobiology: Biological Timekeeping* (Sinauer Associates, Sunderland).
- Santos SD, Verveer PJ, Bastiaens PI (2007) Growth factor-induced MAPK network topology shapes Erk response determining PC-12 cell fate. *Nat Cell Biol* 9:324–330.
- Alon U (2007) Network motifs: Theory and experimental approaches. *Nat Rev Genet* 8:450–461.
- Gardner TS, Cantor CR, Collins JJ (2000) Construction of a genetic toggle switch in *Escherichia coli*. *Nature* 403:339–342.
- Elowitz MB, Leibler S (2000) A synthetic oscillatory network of transcriptional regulators. *Nature* 403:335–338.
- Hasty J, Isaacs F, Dolnik M, McMillen D, Collins JJ (2001) Designer gene networks: Towards fundamental cellular control. *Chaos* 11:207–220.
- Stricker J, et al. (2008) A fast, robust and tunable synthetic gene oscillator. *Nature* 456: 516–519.
- Tigges M, Marquez-Lago TT, Stelling J, Fussenegger M (2009) A tunable synthetic mammalian oscillator. *Nature* 457:309–312.
- Bashor CJ, Helman NC, Yan S, Lim WA (2008) Using engineered scaffold interactions to reshape MAP kinase pathway signaling dynamics. *Science* 319:1539–1543.
- Cağatay T, Turcotte M, Elowitz MB, Garcia-Ojalvo J, Süel GM (2009) Architecture-dependent noise discriminates functionally analogous differentiation circuits. *Cell* 139:512–522.
- Horn HF, Vousden KH (2007) Coping with stress: multiple ways to activate p53. *Oncogene* 26:1306–1316.
- Harris SL, Levine AJ (2005) The p53 pathway: Positive and negative feedback loops. *Oncogene* 24:2899–2908.
- Haupt Y, Maya R, Kazaz A, Oren M (1997) Mdm2 promotes the rapid degradation of p53. *Nature* 387:296–299.
- Lahav G, et al. (2004) Dynamics of the p53-Mdm2 feedback loop in individual cells. *Nat Genet* 36:147–150.
- Geva-Zatorsky N, et al. (2006) Oscillations and variability in the p53 system. *Mol Syst Biol* 2:2006, 0033.
- Batchelor E, Mock CS, Bhan I, Loewer A, Lahav G (2008) Recurrent initiation: A mechanism for triggering p53 pulses in response to DNA damage. *Mol Cell* 30:277–289.
- Loewer A, Batchelor E, Gaglia G, Lahav G (2010) Basal dynamics of p53 reveal transcriptionally attenuated pulses in cycling cells. *Cell* 142:89–100.
- Kaku S, et al. (2001) Binding to the naturally occurring double p53 binding site of the Mdm2 promoter alleviates the requirement for p53 C-terminal activation. *Nucleic Acids Res* 29:1989–1993.
- Wu X, Bayle JH, Olson D, Levine AJ (1993) The p53-mdm-2 autoregulatory feedback loop. *Genes Dev* 7(7A):1126–1132.
- Stommel JM, Wahl GM (2004) Accelerated MDM2 auto-degradation induced by DNA-damage kinases is required for p53 activation. *EMBO J* 23:1547–1556.
- Fang S, Jensen JP, Ludwig RL, Vousden KH, Weissman AM (2000) Mdm2 is a RING finger-dependent ubiquitin protein ligase for itself and p53. *J Biol Chem* 275: 8945–8951.
- Dornan D, et al. (2004) The ubiquitin ligase COP1 is a critical negative regulator of p53. *Nature* 429:86–92.
- Leng RP, et al. (2003) Pirh2, a p53-induced ubiquitin-protein ligase, promotes p53 degradation. *Cell* 112:779–791.
- Tsai TY, et al. (2008) Robust, tunable biological oscillations from interlinked positive and negative feedback loops. *Science* 321:126–129.
- Novák B, Tyson JJ (2008) Design principles of biochemical oscillators. *Nat Rev Mol Cell Biol* 9:981–991.
- Brugnera E, et al. (1994) Cloning, chromosomal mapping and characterization of the human metal-regulatory transcription factor MTF-1. *Nucleic Acids Res* 22:3167–3173.
- Vassilev LT, et al. (2004) In vivo activation of the p53 pathway by small-molecule antagonists of MDM2. *Science* 303:844–848.
- Cai L, Dalal CK, Elowitz MB (2008) Frequency-modulated nuclear localization bursts coordinate gene regulation. *Nature* 455:485–490.
- Shaner NC, et al. (2004) Improved monomeric red, orange and yellow fluorescent proteins derived from *Discosoma sp.* red fluorescent protein. *Nat Biotechnol* 22: 1567–1572.